Proceedings Paper:
Ren, Z, Kashiri, N, Zhou, C orcid.org/0000-0002-6677-0855 et al. (1 more author) (2019) HERI II: A Robust and Flexible Robotic Hand based on Modular Finger design and Under Actuation Principles. In: 2018 IEEE/RSJ International Conference on Intelligent Robots and Systems (IROS). 2018 IEEE/RSJ (IROS), 01-05 Oct 2018, Madrid, Spain. IEEE , pp. 1449-1455. ISBN 978-1-5386-8094-0

https://doi.org/10.1109/IROS.2018.8594507

HERI II: A Robust and Flexible Robotic Hand based on Modular Finger design and Under Actuation Principles

Zeyu Ren, Navvab Kashiri, Chengxu Zhou, Nikos G. Tsagarakis

***Abstract*— This paper introduces the design of a novel under-actuated hand with highly integrated modular finger units, which can be easily reconfigured in terms of finger arrangement and number to account for the manipulation needs of different applications. Each finger module is powered by a single actuator through an under-actuated transmission and equipped with a sensory system for delicate and precise grasping, which includes absolute position measurements, contact pressure sensing at finger phalanxes and motor current readings. Finally, intrinsic elasticity integrated in the transmission system make the hand robust and adaptive to impacts when interacting with the objects and environment. This highly integrated hand (HERI II) was developed for the Centauro Robot to enable robust and resilient manipulation. A set of experiments demonstrating the hand's grasping performance were carried out and fully verified the design effectiveness of the proposed hand.**

I. Introduction

Robotics hands typically function as the end-effector of robotics arms to undertake significant missions for grasping and manipulation. In the past few decades, many multi-fingered robotics hands have been developed for manipulative dexterity, grasping robustness and human operability [1]. They can be classified into two categories based on the Degree of Actuation (DoA): fully-actuated hands [2]–[5], and under-actuated hands [6]–[11]. Despite a set of advantages of fully-actuated hands, such as independent finger joint motion and the ability to mimic most of the sophisticated human hand motions [12], the supremacy of under-actuated hands, in terms of reduced complexity, higher grasping force capacity, simplified control requirements and low cost, have been attracting more and more attention to its development.

The aforementioned different types of under-actuated hands have made great progress in terms of anthropomorphic hardware design in low cost and robust grasping. However, due to the simplification in finger design and reduction in DoA, the majority of under-actuated hands are incapable of executing even basic dexterous motions such as pinching, triggering and thumb abduction/adduction. Furthermore in most under-actuated hands, the mechanical transmission system couples one actuator to several fingers, such a coupling adds complexity in the transmission routing, reduces the robustness and mechanical efficiency as well as hinders the regular maintenance.

Motivated by the limitations of under-actuated hands, we developed a novel hand design in such a way that the finger distribution and quantity could be configured based on different application requirements. Moreover, the mechanical transmission between the under-actuated finger and the actuator is designed to deliver high efficiency and maintenance convenience. To achieve the configurable finger distribution and quantity, and improve the electronics/mechanics integration of the whole hand, fingers are designed to be as an independent and identical modules with individual actuation. Since the grasping algorithms and kinematics analysis for the under-actuated finger are highly depend on its structure, the utilisation of identical finger modules will improve the standardisation of hardware and facilitate the general applicability of different grasping algorithms.

The authors are with Humanoid and Human Centered Mechatronics Research Line, Istituto Italiano di Tecnologia, via Morego, 30, 16163 Genova, Italy. E-mail: zeyu.ren@iit.it

(a) A four-finger configuration (b) A three-finger configuration

Fig. 1: HERI II Hand in two configurations.

The rest of the paper is organised as follows: Section II explains the conceptual design of HERI II Hand. Section III details the mechanical design of the finger module and integration features. In Section IV, series of experiments carried out to demonstrate the performance of the design are described. In Section V, the performance of the HERI II hand in comparison with the previous generation HERI Hand [9] is conducted. The summary for the current results and future work plan are eventually presented in Section VI.

II. Conceptual Design

In this section, the design concept of the finger quantity and distribution of the proposed hand based on the finger module utilisation is detailed.

For the under-actuated hand, the finger quantity and distribution could possess several arrangements [7]–[9], which depend on the specific applications and requirements. From the bionic engineering view, the most preferable solution for the finger quantity and distribution of a robotic hand would be as identical as a human's hand. However, due to space limitation and high complexity, very few designs of under-actuated hands follow completely the bionic configuration and most decisions for the finger quantity and distribution

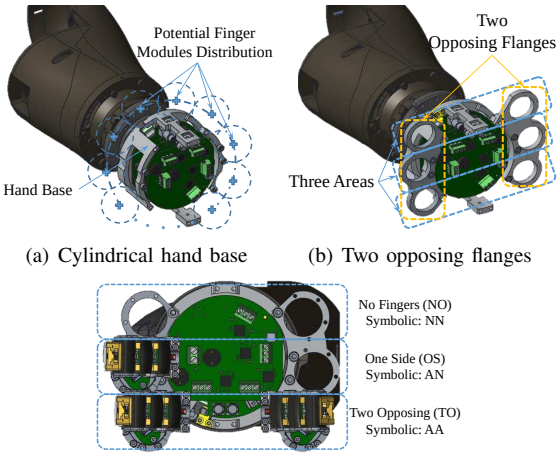

(a) Cylindrical hand base (b) Two opposing flanges

(c) Example for three kinds of finger arrangement

Fig. 2: Scheme for finger module arrangement.

TABLE I: Functionality and cost related figures for the three types of finger arrangement in one dashed blue area.

Finger Arrangement	Symbolic(1)	Corresponding Performance Score			
		Robust grasping	Pinch	Trigger	Economic
None (NO)	NN	0	0	0	1
One-Side (OS)	AN or NA	1	0	1	1
Two-Opposite (TO)	AA	1	1	1	0

Note: (1) We use **A** to represent the equipment of finger module at either location in one opposing flange and **N** to represent not equipped.

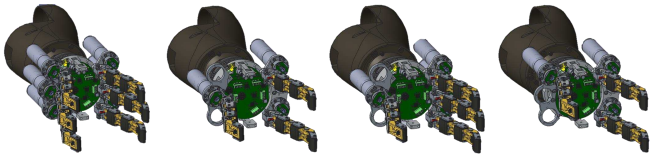

(a) (b) (c) (d)

Fig. 3: Four types of common finger configuration examples of HERI II Hand.

are the results of trades off among different proposals based on different functionality priorities [9]. One of the important property of HERI II Hand is its configurable finger quantity and arrangement, which means that the specific finger quantity and distribution can be adjusted according to different manipulation requirements. The precondition for the configurable feature is that each finger needs to be identical, modular and absolutely independent to each other.

The desired hand base is designed as a cylinder, hence the finger modules can be freely distributed around the cylindrical base as shown in Fig. 2(a). Considering placing the fingers opposite to each other is necessary to realise finger pinch manipulation [13]. Two opposing flanges for fixing six finger modules are designed as Fig. 2(b) shows, where the two opposing flanges can be divided into three areas for placing finger modules opposite to each other.

For the selection of the arrangement for the finger modules in the two opposing flanges, let consider the three distinct areas of the hand base as shown by the dashed blue lines in Fig. 2(c). Each of these three areas can be equipped with one finger at one side (OS), two opposing fingers (TO) or eventually with no fingers (NO). The provided manipulation functionality for each of these cases is reported in Table I where a consideration related to the cost is also detailed.

Several possible finger configurations for composing the whole hand with their corresponding performance scores are presented in Table. II, where it can be seen that different finger configurations provide different level of functionality and advantages. HERI II Hand can be configured based on different requirement priority. For instance,

- If the hand is desired for pinch motion, especially for the long cylinder object, the configuration $[AA, AA, AA]^T$ should be adopted as shown in Fig. 3(a);
- If the hand is supposed to do the robust grasping considering also the cost, the configuration $[NA, AN, NA]^T$ could be utilised as presented in Fig. 3(b);
- If the hand is designed to achieve a relative balance performance between pinch, robust grasping, trigger and in low cost, the configurations $[NA, AA, NA]^T$ or $[AA, NN, NA]^T$ could be chosen as Fig. 3(c) and 3(d) demonstrate.

In this work and for the application of this hand to the Robot [14] [15], the functionalities of robust grasping, precise pinch and trigger motion in low cost are desirable. As a result, the configurations $[NA, AA, NA]^T$ and $[NA, AN, NA]^T$ shown in Fig. 1(a) and 1(b) were adopted as the current hardware realisation.

III. Design Specifications

In this section, the finger module design principles of HERI II Hand in terms of phalanx design, motor selection, tendon transmission, sensor configuration, passive compliant structure and finger release elastic element are detailed. Meanwhile the integration property of embedded electronics and the 6-axis Force/Torque sensor are also described.

A. Finger Module Design

The hand design relies upon modular fingers with identical feature. Fig. 4 shows a CAD image of the modular finger. The main features resulting in the desired finger modular design will be presented as follows:

TABLE II: Several possible whole hand finger configurations and corresponding performance score.

Finger Configurations(1)	Desired Whole Hand Score			
	Robust grasping	Pinch	Trigger	Economic
$[AA, AA, AA]^T$	3	3	3	0
$[AA, NA, AA]^T$	3	2	3	1
$[AA, NN, AA]^T$	2	2	2	1
$[NA, AA, NA]^T$	3	1	3	2
$[AA, NA, NN]^T$	2	1	2	2
$[NA, AN, NA]^T$	3	0	3	3

Note: (1) We utilise the transpose of a 3×1 Matrix to describe the whole hand configuration based on three types of finger arrangement in Table I.

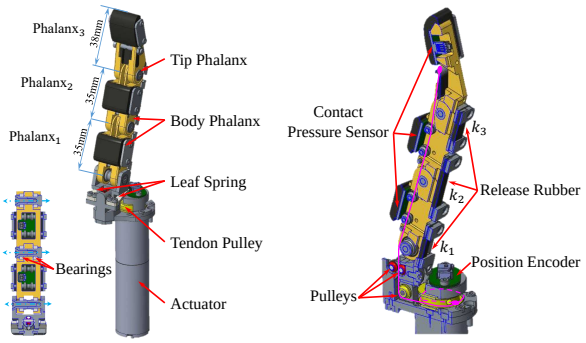

(a) (b)

Fig. 4: Finger module design with components annotated.

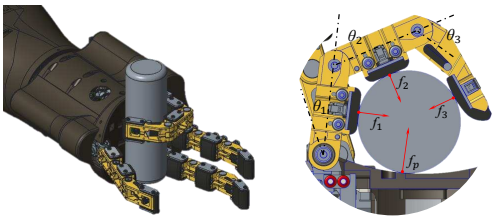

(a) 40mm diameter cylinder (b) Force analysis

Fig. 5: Proposed grasping scenario of single finger.

1) Finger and Phalanx Design: The design of an individual finger module, particularly the set of phalanxes, follows the same concept as the first version of the HERI Hand, see [9] for the design details. However, the length of body and tip phalanxes, as illustrated in Fig. 4(a), is adjusted to reduce the overall length of the hand, and therefore lead to a more compact hand proportional in size to the Centauro forearm presented in [14]. The body and tip phalanxes are 35 and 38 mm long respectively, so that the overall finger length is approximately 100 mm in extension condition.

2) Actuator Selection: As the grasping performance of under-actuated fingers, and the corresponding contact forces generated on the phalanxes, depends non-negligibly on the profile of the grasped objects, the selection of the actuator requires an exemplary grasping scenario. To this end, we target grasping a cylindrical object of 40 mm diameter and 1.0 kg mass using the proposed finger module. Fig. 5(a) shows the scenario, and Fig. 5(b) presents the corresponding force analysis information, where f_1, f_2 and f_3 show the force applied to the object by the phalanxes while f_p represents the force applied by the hand palm.

We utilise the relationship between the phalanx contact forces $\boldsymbol{f} = [f_1, f_2, f_3]^T$ and the finger joint torques $\boldsymbol{\tau}(\tau_m) = [\tau_1, \tau_2, \tau_3]^T$ for the three-phalanx under-actuated finger, with τ_m indicating the finger motor torque. It can be shown by

$$\boldsymbol{f} = \mathbf{J}^{-\mathrm{T}}\mathbf{H}^{-\mathrm{T}}\boldsymbol{\tau}. \tag{1}$$

where $\mathbf{J}$ and $\mathbf{H}$ symbolise the corresponding Jacobin and transmission matrices as detailed in [9], [16].

According to the static force balance of the gasped object w.r.t. the hand, we can show $f_p = \boldsymbol{F}^T(\theta_1, \theta_2, \theta_3)\boldsymbol{f}$ where $\boldsymbol{F}$ symbolises the appropriate force balance vector. Using this relation to augment (1), we can extract the maximum payload of the finger M_{max} in the worst holding posture, i.e. when the finger closing plane is perpendicular to the gravity vector as follows

$$M_{max}g = \boldsymbol{\mu}^T \begin{bmatrix} \mathbf{I} \\ \boldsymbol{F}^T \end{bmatrix} \mathbf{J}^{-\mathrm{T}}\mathbf{H}^{-\mathrm{T}}\boldsymbol{\tau}, \tag{2}$$

where $\boldsymbol{\mu} = [\mu_1, \mu_2, \mu_3, \mu_p]^T$ represents the vector of friction coefficients between the object and phalanxes/palm, $\mathbf{I}$ shows the identity matrix of dimension 3×3, and g is the gravitational acceleration.

The required motor torque can be then obtained by solving (2) for τ_m which is embedded in the joint torque vector $\boldsymbol{\tau}$. For the aforementioned target object the required motor torque is computed as follows. Using the geometry of the hand and the object, the finger posture is found as $\theta_1 = 24°$, $\theta_2 = 60°$ and $\theta_3 = 54°$. To proceed with the actuator selection, we also consider the stiffness of the opposing joint springs that are realised by the release rubber elements and set on the basis of the weight of phalanxes as $k_1 = 0.08$, $k_2 = 0.12$ and $k_3 = 0.16$ Nm/rad, see [9] for details. To account for the worst case scenario, we assume low friction coefficient between the hand phalanxes/palm and object surface selecting $\mu_i = 0.2$ for $i = 1, 2, 3, p$. Moreover, the motor and mechanical transmission efficiency were set to $\eta_m = 0.5$ and $\eta_t = 0.45$, respectively. The required motor torque is therefore calculated to be approximately equal to 3 Nm. Therefore we selected Maxon DCX22L motor with the gear ratio of 138 that can deliver a continuous output torque of 3.3 Nm and a maximum velocity of 7.6 rad/s.

3) Tendon Transmission: We adopt the classic *Da Vinci's Mechanism* [16] approach for the transmission system of the under-actuated finger to render flexion motion as shown in Fig. 4(b). Multiple pulleys supported by miniature bearings are utilised to guarantee the smooth tendon route, thereby enhancing the endurance and reliability of the grasping performance by reducing friction and wearing in the tendon transmission. Based on the selected motor and the motor output tendon pulley of 8 mm radius, the maximum linear force applied on the tendon can reach up to 475 N. As a result, we select LIROS DSL of 0.7 mm diameter with polyester cover material and dyneema core as the transmission tendon, which can resist up to 700 N linear force to account for a safety factor of 1.5 approximately.

To ensure the robustness of tendon transmission, contacts of the tendon with any surfaces but pulleys have been eliminated. As the tendon connects the finger tip to the motor output pulley, it is essential to provide the end-points with smooth and robust connections. While robust connection of tendon to output pulley is achieved via a through hole along the pulley diameter, attachment to the finger tip is carried out by a noose knot tying the tendon to a pin at the finger tip, see Fig. 6(a). Furthermore a rubber in hardness shore A65 is utilised inside the fingertip as a spring-damper in series with the tendon enabling to absorb impact/abrupt forces at the finger by holding the aforementioned pin .

4) Sensor Configuration: The sensory components of the finger module are presented in Fig. 4(b). In addition to the motor currents that are monitored to estimate the torque applied by motors, an on-axis magnetic encoder is utilised for measuring the absolute position of the motor output pulley. We selected a 14-bit AMS position sensor providing an angle measurement resolution of 0.022° for the motor pulley displacement. Moreover, a set of custom tactile/contact pressure sensors, developed on the basis of a resistive sensing principle [17], are employed to measure the vertical component of the external force on finger phalanxes. Each pressure sensor circuit board is covered by a rubber layer for boards protection and also providing the hand with compliant contact points and increased grip during grasping.

5) Passive Compliant Roll Joint: While human fingers can actively control both pitch and roll motions, under-actuated hands can mostly render the primary pitch motions. As a result, while the phalanx structure of under-actuated hands do not often suffer from impact damage in the finger flexion-extension motion plane due to passive degrees of freedom in this plane, the finger design is often rigid in the adduction-abduction plane and can be damaged when subject to impacts in this plane. To escalate the robustness of the finger module, it is essential to overcome the rigidity of the finger in adduction-abduction plane without increasing the actuation and structure complexity. We therefore introduce a spring loaded passive roll joint at the base of the finger unit as shown in Fig. 6(b). We limit the deflection range to $\theta_r = \pm 5^\circ$ through mechanical limitation, and target a desired stiffness of $k_r = 15\,\text{Nm/rad}$ for this compliant joint, thereby standing over 1 kg at the finger tip without reaching full deflection. Fig. 6(b) shows the corresponding forces on the finger module. The torque τ_r on the roll joint is given by

$$\begin{aligned} \tau_r &= k_r \cdot \theta_r \\ &= f_t \cdot l_t = f_l \cdot l_l, \end{aligned} \tag{3}$$

where l_t and l_l are the finger tip length and leaf spring lever length respectively, and f_t and f_l are the forces associated with these locations. When the maximum deflection of the joint occurs, the aforesaid stiffness generates $f_l = 130.5\,\text{N}$ on the leaf spring, corresponding to $f_t = 11.9\,\text{N}$, considering that the relevant lengths are $l_l = 10\,\text{mm}$ and $l_t = 110\,\text{mm}$. A leaf spring in accordance with the aforesaid specifications in terms of stiffness and strength, as well al compatible with available space, is therefore designed, on the basis of a clamp-free cantilevered beam concept. The placement of the two leaf springs, for replicating compliance in two directions, is shown in Fig. 6(b). The Finite Element Method (FEM) analysis results of the beam, including strain, stress and displacement, are presented in Fig. 7, where 17-4PH H900 steel was selected as the leaf spring material. The Stiffness of the final design is therefore obtained as 13.2 Nm/rad.

6) Finger Release Elastic Element: Since the tendon transmission according to *Da Vinci's Mechanism* approach can not apply force for finger release, as elaborated in [16], it is essential to design a set of elastic elements for

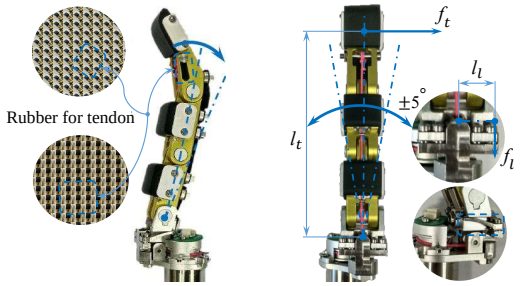

(a) Damping rubber design (b) Leaf spring design

Fig. 6: Compliant structure in (a) pitch and (b) roll direction.

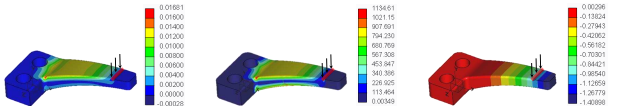

(a) Strain (b) Stress (MPa) (c) Displacement (mm)

Fig. 7: FEM analysis for leaf spring of finger module.

finger phalanx joints to release the finger (extension motion) when finger closing (flexion motion) is not intended/applied. We adopt the elastic rubber of different stiffness level for each phalanx joint, instead of extension springs used in the first version of the hand presented in [9], since it allows fine tuning of the joint stiffness. Furthermore, the rubber's superior damping performance decreases the finger tremble in real applications. The rubber element and its mounting on the the finger is shown in Fig. 8, where the different stiffness of each joint is achieved by clamping the rubber at two different sections of the rubber. The rubber used in the finger module, when clamped as shown in Fig. 8, renders three stiffness values of 880, 950, 1660 N/m from base to tip, that correspond to $k_1 = 0.071$, $k_2 = 0.077$ and $k_3 = 0.134\,\text{Nm/rad}$, closely matching the values used for the actuator selection analysis.

B. Integrated Hand Design

Since the proposed hand is developed as an end-effector for the Centauro Robot [14], we adapt the design with the robot forearm in a way that a compact design embodying essential components is achieved. Fig. 9 reveals the HERI II Hand's integration with the Centauro forearm. Starting from the forearm wrist rotation interface, we integrate a 6-axis F/T sensor for connecting the wrist interface to the hand. The hand unit includes a basement part on which all the finger modules, palm and covers are mounted. It

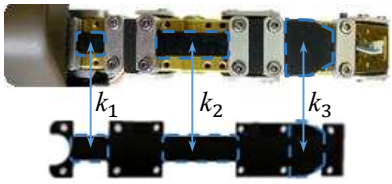

Fig. 8: Finger release elastic element design.

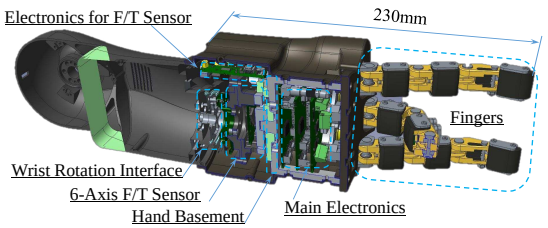

Fig. 9: HERI II Hand cross section showing the integration of the various electronics and F/T sensor.

TABLE III: HERI II Hand and finger module specifications.

	HERI II Hand in Fig. 1(a) Configuration
Weight	1.6 kg
Overall Dimension	230 mm × 105 mm × 105 mm
	Finger Module
Motor Type	Maxon DCX22L GB KL 48V
Gearbox Type	Maxon Planetary GPX22HP 138:1
Continuous Torque	3.3 Nm
Tendon Guidance Pulleys Number	8
Estimated Transmission Efficiency	$\eta_m = 0.5$, $\eta_t = 0.45$
Tendon Transmission Length	126 mm
Tendon Material	LIROS DSL 0.7 mm
Sensor Configuration	Position & Contact Pressure Sensors, Current Reading
Release Rubber Stiffness(1)	$k_1 = 880$ N/m, $k_2 = 950$ N/m, $k_3 = 1660$ N/m
Weight	298 g

Note: (1) The rubber sheet is from MISUMI RBCM2-20, the different stiffness is achieved by cropping into different sectional area.

contains the electronics to drive the finger motors and read the sensors including the F/T sensor and the fingers' sensory data. The specifications of the proposed hand integrated into the Centauro robot [14] forearm is reported in Table III.

IV. Experimental Evaluation

To verify the hand performance, a series of experiments were performed on the hand.

A. Robust Grasping Performance

The first experiment evaluates the whole hand vertical grasping performance. As shown in Fig. 10(a), the hand is able to vertically grasp a cylinder object of 75 mm diameter and 4354 g weight. Meanwhile all the corresponding contact pressure at the phalanxes of four fingers during the experiment are presented from Fig. 10(b)-10(e), where the specific finger naming order could be refer from Fig. 10(a).

The measured contact forces from corresponding finger phalanxes possess variation during grasping and meanwhile slightly differ from theoretical calculated forces, which can be observed from Fig. 10(b)-10(e). The two main potential reasons are as following,

- The contact configuration and pressure may not the same in all fingers and depends on the placement of the object in the hand with respect to the fingers;
- The external disturbance applied on the under-actuated finger during grasping from adding weights will result in the posture variation of the finger [18], which will eventually change the contact forces in the fingers.

Another experiment was performed by controlling the hand to grasp a hammer and execute the task of knocking a nail in a wood block as depicted in Fig. 11(a). The disturbance during knocking nail applied on four fingers can

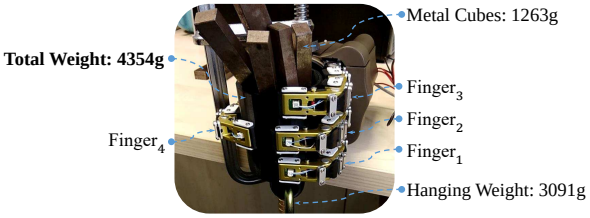

(a) Vertical grasping experiment and finger naming order

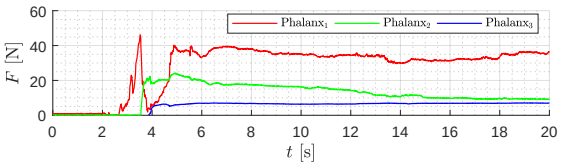

(b) Finger$_1$ contact force curve

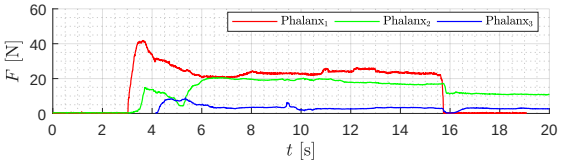

(c) Finger$_2$ contact force curve

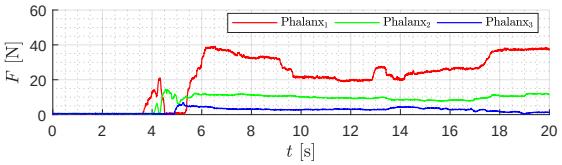

(d) Finger$_3$ contact force curve

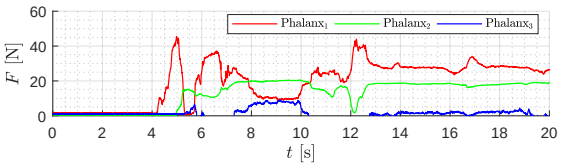

(e) Finger$_4$ contact force curve

Fig. 10: Robust grasping experiment of vertically holding a cylinder object in 4354 g weight.

be detected from contact force curves in Fig. 11(b)-11(e). The impact effects can be obviously noticed on Finger$_1$ as shown in Fig. 11(b), demonstrating the robust grasping of the proposed hand and its physical resilience to impacts.

B. Dexterous Manipulation Performance

The dexterous performance of the hand is firstly demonstrated by holding the drill and repeatedly triggering the power on button, which fully utilised the dexterous property in terms of controlling each finger module independently.

As shown in Fig. 12(a), the progress of repeatedly triggering Bosch drill is demonstrated and the corresponding contact force curves of four fingers during the experiment are shown from Fig. 12(b)-12(e). From Fig. 12(d) we can observe two peak contact force curves from Finger$_3$, which is the finger we controlled to press the trigger button twice. Fig. 12(f) demonstrates the curves of reference and measured

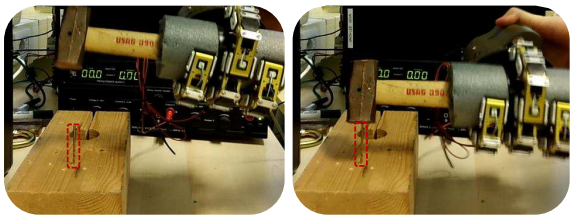

(a) Knocking nail experiment

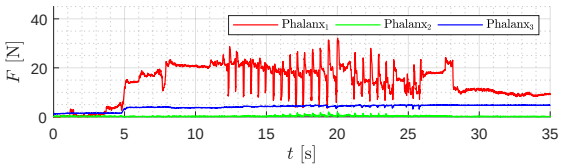

(b) Finger$_1$ contact force curve

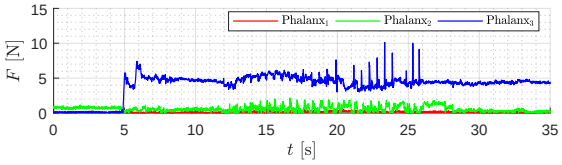

(c) Finger$_2$ contact force curve

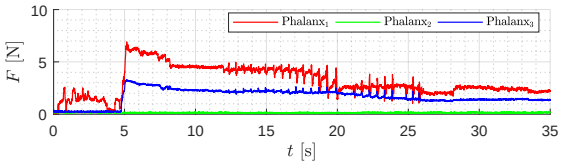

(d) Finger$_3$ contact force curve

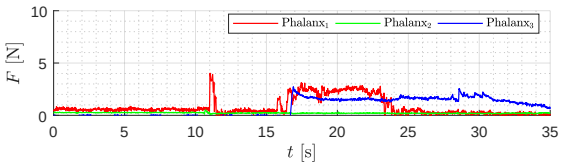

(e) Finger$_4$ contact force curve

Fig. 11: Powerful grasping a hammer during the high impact knocking nail task.

absolute position of the tendon displacement for driving the under-actuated finger. The position steps are at 9 s and 15 s in Fig. 12(f), is evident and correspond to the two triggers motions. The vibration from working drill during the first trigger, caused change in the drill grasping posture. Finger$_1$, Finger$_2$ and Finger$_4$ were used to grasp the drill tighter in order to successfully realise the second trigger. As the drill button location with respect to the finger performing the trigger slightly changed during the second tighter grasping, the reference position of Finger$_3$ for second trigger was increased for ensuring success as shown in Fig. 12(f), which naturally leads to the bigger contact force on finger$_3$ as presented in Fig. 12(d). Finally the currents for driving the motors of four fingers are plotted in Fig. 12(g).

The second part of this experiment evaluated the pinch functionality of the $[NA, AA, NA]^T$ finger configuration adopted for the hand in this work. In particular the hand was controlled to precisely pinch objects on the table, such as a small coin and a pen as presented in Fig. 13(a) and 13(b) respectively.

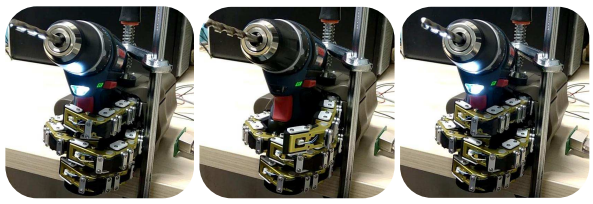

(a) Repeatable trigger experiment

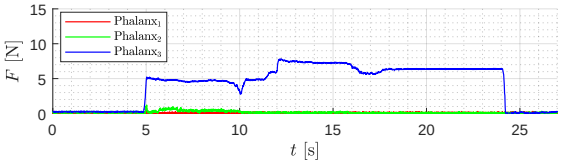

(b) Finger$_1$ contact force curve

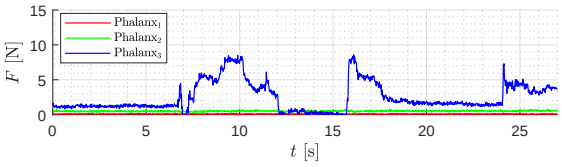

(c) Finger$_2$ contact force curve

(d) Finger$_3$ contact force curve

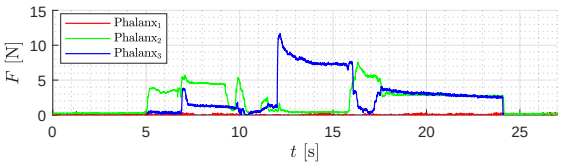

(e) Finger$_4$ contact force curve

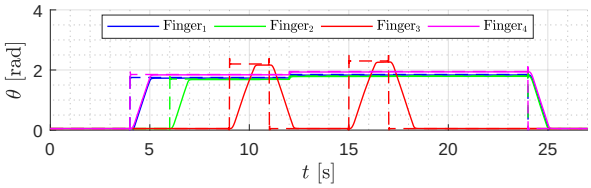

(f) Reference position curve (dashed line) and measured position curve (solid line) of four tendon displacements for finger flexion

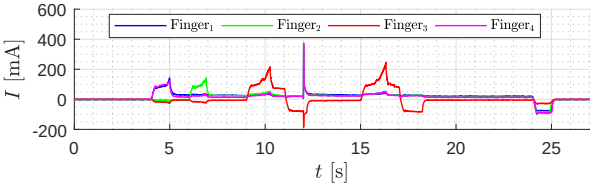

(g) Current curve of four motors

Fig. 12: Dexterous manipulation of trigger drill repeatedly.

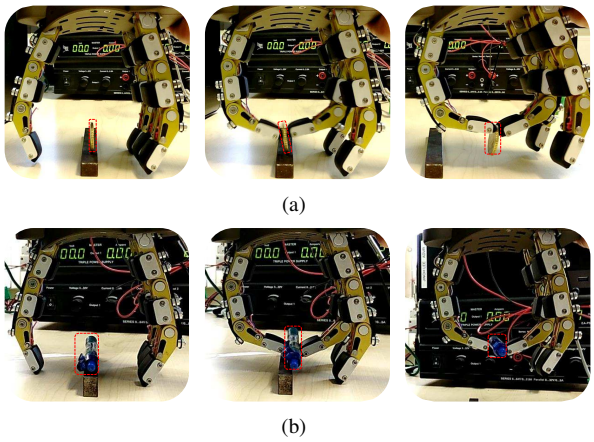

(a)

(b)

Fig. 13: Precisely pinch (a) a coin and (b) a pen from table.

V. Discussion

The performance comparison between HERI II Hand and HERI Hand [9] will be discussed in following two aspects.

- The weight-grasping ratio of HERI II hand is 2.716, which is 2.2 times higher of that (1.218) of HERI Hand weight-grasping ratio in terms of vertical grasping ability. The HERI Hand weights 1190 g mass and can hold a 1450 g weight while the revised HERI II Hand has a mass of 1603 g and is able to hold a 4354 g weight.
- Compared to HERI Hand, the reliability in mechanical transmission has been significantly improved thanks to the simplification of the tendon route through the modular finger design. This also improved the integration of various mechanical components and electronics enhancing the maintenance efficiency of the entire hand hardware.

VI. Conclusion & Future Work

In this paper, we proposed the design of a novel under-actuated hand based on highly modular finger units. Each finger module is equipped with the corresponding actuator, under-actuated transmission, and sensors in compact integration. For each finger module, the tendon route is reasonably simplified for ensuring the reliability. To allow the manipulation monitoring and control, full sensory feedback of finger modules are provided. This includes absolute position measurements, contact pressure sensing at the finger phalanxes and motor current readings. Intrinsic elasticity integrated in the transmission system make the hand robust and adaptive to impacts when interacting with the objects and environment. The advantages of applying finger module concept in under-actuated hands are the robust grasping and dexterous performance as well as the maintenance convenience. The hand is able to stably grasp and hold an object of 4354 g in weight and perform hammering of a nail. The dexterous performance was demonstrated by triggering a Bosch drill and precisely pinching small objects from the table. Finally the ability of the sensory system of the hand in providing indications of the contacts and the applied forces in the finger phalanxes was confirmed. More work regard to the potential of the hand in different finger configurations as well as more dedicated grasping control strategies based on the pressure sensor feedback will be explored.

Acknowledgement

This work is supported by European's H2020 robotics project CENTAURO (644839) and CogIMon (644727).

References

[1] A. Bicchi, "Hands for dexterous manipulation and robust grasping: A difficult road toward simplicity," *IEEE Transactions on robotics and automation*, vol. 16, no. 6, pp. 652–662, 2000.

[2] S. C. Jacobsen, J. E. Wood, D. Knutti, and K. B. Biggers, "The UTAH/MIT dextrous hand: Work in progress," *The International Journal of Robotics Research*, vol. 3, no. 4, pp. 21–50, 1984.

[3] M. Grebenstein, M. Chalon, G. Hirzinger, and R. Siegwart, "Antagonistically driven finger design for the anthropomorphic DLR hand arm system," in *IEEE-RAS International Conference on Humanoid Robots*, 2010, pp. 609–616.

[4] G. Palli, C. Melchiorri, G. Vassura, U. Scarcia, L. Moriello, G. Berselli, A. Cavallo, G. De Maria, C. Natale, S. Pirozzi *et al.*, "The DEXMART hand: Mechatronic design and experimental evaluation of synergy-based control for human-like grasping," *The International Journal of Robotics Research*, vol. 33, no. 5, pp. 799–824, 2014.

[5] A. Kochan, "Shadow delivers first hand," *Industrial robot: an international journal*, vol. 32, no. 1, pp. 15–16, 2005.

[6] M. G. Catalano, G. Grioli, E. Farnioli, A. Serio, C. Piazza, and A. Bicchi, "Adaptive synergies for the design and control of the Pisa/IIT softhand," *The International Journal of Robotics Research*, vol. 33, no. 5, pp. 768–782, 2014.

[7] K. Mitsui, R. Ozawa, and T. Kou, "An under-actuated robotic hand for multiple grasps," in *IEEE/RSJ International Conference on Intelligent Robots and Systems*, 2013, pp. 5475–5480.

[8] R. R. Ma, L. U. Odhner, and A. M. Dollar, "A modular, open-source 3d printed underactuated hand," in *IEEE International Conference on Robotics and Automation*, 2013, pp. 2737–2743.

[9] Z. Ren, C. Zhou, S. Xin, and N. Tsagarakis, "HERI Hand: A Quasi Dexterous and Powerful Hand with Asymmetrical Finger Dimensions and Under Actuation," in *IEEE/RSJ International Conference on Intelligent Robots and Systems*, 2017, pp. 322–328.

[10] L. Wang, J. DelPreto, S. Bhattacharyya, J. Weisz, and P. K. Allen, "A highly-underactuated robotic hand with force and joint angle sensors," in *IEEE/RSJ International Conference on Intelligent Robots and Systems*, 2011, pp. 1380–1385.

[11] A. Edsinger-Gonzales, "Design of a compliant and force sensing hand for a humanoid robot," DTIC Document, Tech. Rep., 2005.

[12] P. Tuffield and H. Elias, "The shadow robot mimics human actions," *Industrial Robot: An International Journal*, vol. 30, no. 1, pp. 56–60, 2003.

[13] T. Feix, J. Romero, H.-B. Schmiedmayer, A. M. Dollar, and D. Kragic, "The grasp taxonomy of human grasp types," *IEEE Transactions on Human-Machine Systems*, vol. 46, no. 1, pp. 66–77, 2016.

[14] L. Baccelliere, N. Kashiri, L. Muratore, A. Laurenzi, M. Kamedula, A. Margan, S. Cordasco, J. Malzahn, and N. G. Tsagarakis, "Development of a human size and strength compatible bi-manual platform for realistic heavy manipulation tasks," in *IEEE/RSJ International Conference on Intelligent Robots and Systems*, 2017.

[15] L. Muratore, A. Laurenzi, E. M. Hoffman, A. Rocchi, D. G. Caldwell, and N. G. Tsagarakis, "Xbotcore: A real-time cross-robot software platform," in *IEEE International Conference on Robotic Computing (IRC)*. IEEE, 2017, pp. 77–80.

[16] L. Birglen, T. Laliberté, and C. M. Gosselin, *Underactuated robotic hands*. Springer, 2007, vol. 40.

[17] K. Weiß and H. Worn, "The working principle of resistive tactile sensor cells," in *IEEE International Conference on Mechatronics and Automation*, vol. 1. IEEE, 2005, pp. 471–476.

[18] R. Balasubramanian, J. T. Belter, and A. M. Dollar, "External disturbances and coupling mechanisms in underactuated hands," in *ASME 2010 International Design Engineering Technical Conferences and Computers and Information in Engineering Conference*. American Society of Mechanical Engineers, 2010, pp. 175–184.